Journal of the Earth and Space Physics, Vol. 43, No. 4, Winter 2018, P. 11-26

Analysis of Low-Frequency Passive Seismic Attributes in Maroun Oil Field, Iran

Ebrahimi, M.[1], Moradi, A.[2*] and Seidin, H.[3]

1. M.Sc., Department of Seismology, Institute of Geophysics, University of Tehran, Iran
2. Assistant Professor, Department of Seismology, Institute of Geophysics, University of Tehran, Iran
3. M.Sc., R&D Geophysicist in NIOCEXP, National Iranian Oil Company (NIOC), Tehran, Iran

(Received: 1 Oct 2016, Accepted: 24 Oct 2017)

Abstract

Nowadays, viable and cost-effective methods play a vital role in hydrocarbon exploration up to the point that geoscientists cannot rule out the importance of the passive seismic method (PSM) in oil exploration operations. This method is based on seismic energy, which has a natural source. This study focuses on seismic energy anomaly of 1-6 Hz. Some researches show that spectral and polarization analysis in low-frequency of seismic noises can be used in determining the location of hydrocarbon reservoir. In this paper, these methods were used in Maroun oil field. Using the seismic data recorded by five seismometers, Vertical-to-Horizontal spectral ratio (V/H), Power Spectral Density (PSD) and polarization analysis were studied in the mentioned area. Based on the results, these microtremors can be used as a hydrocarbon indicator. In this study, transient and artificial noises are removed from raw data with various techniques. Afterward, the vertical-to-horizontal spectral ratio method was used and the results were analyzed and compared. Subsequently, the PSD method was investigated and its results were compared with each other at different stations. Following this, polarization analysis was considered that was normally followed by parameters such as strength, dip, rectilinearity and azimuth in particular. Results showed that MAR5 Station was placed over an area with hydrocarbon potential and there are medium to low hydrocarbon potentials at other stations. There is also a positive correlation between passive seismic analysis and the result of seismic reflection surveys carried out in the earlier studies.

Keywords: Passive Seismic, Maroun oilfield, Spectral analysis, Polarization analysis, PSD.

1. Introduction

Dangel et al. (2003) first reported spectral ratio to explore hydrocarbon reservoir anomaly. Such anomalies in the range frequency of 1-6 Hz for proportional vertical spectrum are compared to that of surrounding areas. Passive seismic techniques are relatively new, and a consensus on terminology among interested groups worldwide has not been reached (Asten, 2006).

The major sources of ambient noise lower than 1 Hz called microseism that are due to large-scale meteorological events and oceanic waves. Ambient noises higher than 1 Hz are generated from urban areas, vehicle traffic, railways, machinery, natural sources and noises generated by wind in remote locations (high-frequency noise). Ambient noise from such sources propagates principally as surface waves (Gerivani et al., 2012; Marzorati and Bindi, 2006; Peterson, 1993; Webb, 2007; Wilson et al., 2002; Young et al., 1996). Furthermore, ambient noise with special characteristics has also been observed over the hydrocarbon reservoirs (Saenger et al., 2007a).

A growing number of techniques, ranging from spectral to polarization indicators, have been developed to analyze hydrocarbon microtremor signals to provide information about the presence of hydrocarbon reservoir (Dangel et al., 2003; Holzner et al., 2005).

The peak of the vertical component spectrum in the range frequency of 1-6 Hz was studied by Walker (2008). Seismic waves passing through the hydrocarbon reservoir are recorded with a low frequency of 1-6 Hz. The distribution of anomaly over the hydrocarbon reservoir and under the stations can be obtained by investigating the amplitude spectrum of vertical-to-horizontal spectral ratio, using the recorded waveforms of seismometer over the reservoir, its surroundings and their comparison to each other.

In diverse oil and gas fields throughout the world, passive seismic studies report positive

*Corresponding author: asmoradi@ut.ac.ir

correlation between low frequency spectral anomaly and spatial location of hydrocarbon reservoir (Dangel et al., 2003; Holzner et al., 2005; Lambert et al., 2009; Saenger et al., 2007c).

In this study, the spectral analysis was used to interpret spatial variation associated with a hydrocarbon reservoir prospect. As far as polarization is concerned, the analysis of particle motion as a function of time is described as the polarization analysis (Jurkevics, 1988). This indicator plays a vital role in the identification of hydrocarbon potential, that is also used in this study.

2. Geology and Seismicity

Khuzestan plain over Maroun oil field is located in the south-western part of Zagros fold-thrust belt. The Zagros folded belt lies on the northern margin of under-thrusting Arabian continental crust, above a Precambrian metamorphic basement (Berberian, 1986).

The sedimentary rocks of Zagros are mainly shelf type. Sediments from Zagros mountain range have been deposited on the subsiding basement of the Arabian continental margin from late Precambrian to Miocene time.

The sedimentary section, relatively thick (about one km) Infra-Cambrian evaporates facie and salt deposit of the Hormoz series from Miocene section, for the most part is continuous. Numerous plastic layers of evaporate and salt deposits are also present in the Mesozoic sedimentary section (Jackson and McKenzie, 1984).

The total thickness of sedimentary cover varies between nearly 5 to 10 km (Berberian, 1995). The moderate to large magnitude earthquakes in meizoseismal area are localized and concentrated along particular structural geomorphologic features that contain some major hydrocarbon fields, especially Maroun oil field, throughout the world. The sedimentary column of the area comprises of a ~ 12 km thick section of lower Cambrian through Pliocene strata without significant angular unconformities.

Believed to be involved in the fold-thrust belt, the oldest sedimentary unit is the late Proterozoic to early Cambrian. The Hormoz salt is overlain by 6-10 km of platformal deposits including shale, dolomite and predominantly sandstone, in the Cambrian through Triassic section and limestone in the Jurassic Lower Miocene section (Jackson, 1980; Jackson and Fitch, 1981).

Regarding Maroun as a part of Khuzestan plain, Zagros folded belt has a strong effect on the seismicity of this zone. Due to a highly plastic layer named Hormoz salt formation, this area is one of the most seismically-active belts in Asia (Berberian, 1981, 1995).

3. Measurements

Data acquisition in Maroun oil field was done by five temporary Seismic Network stations in December 2005. The local Seismic Network in Maroun consists of four short-period GBV (MAR1-4 stations) and one Broad-Band GURALP seismometer (MAR5 station). The continuous time-series data recorded by all five stations was visually inspected. The locations of these five stations are shown in Table 1 and Figure1.

Table 1. Location of field stations and their subsoil conditions.

Station	Village Name	Latitude	Longitude	Elevation	Soil Conditions
MAR1	Sudan	31º05.2′	49º16.5′	33.0	Alluvium and Neighbored by Aghajari Formation
MAR2	Mosharafeh-e Kuchak	31º08.7′	49º13.6′	51.6	Alluvium and Neighbored by Aghajari Formation
MAR3	Beit-e Savadi	31º11.8′	49º18.1′	77.0	Alluvium
MAR4	Alvan Moslem	31º07.1′	49º22.8′	106.9	Alluvium
MAR5	Owdeh	31º16.7′	49º07.9′	53.2	Alluvium

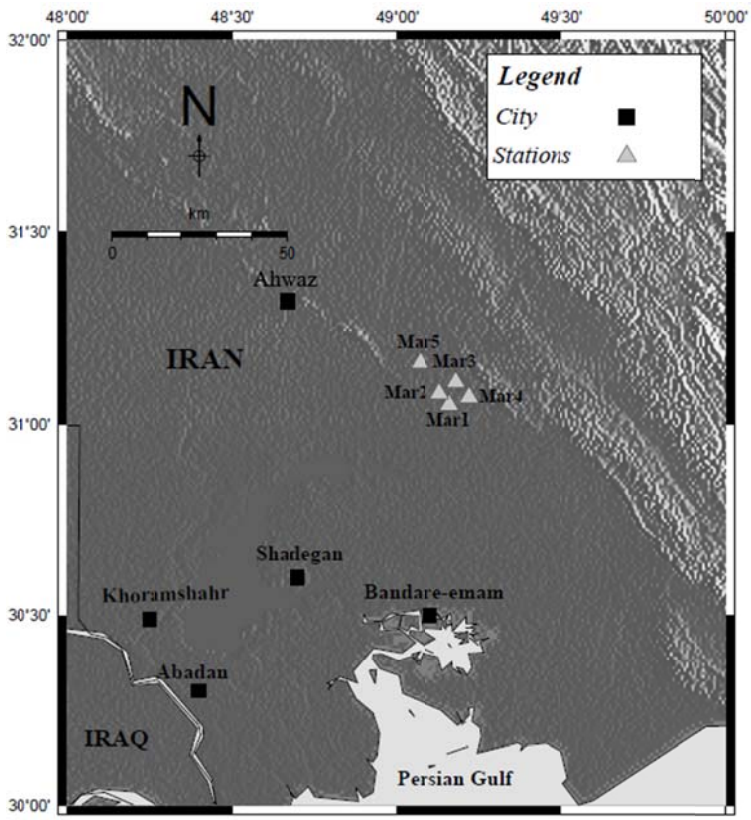

Figure 1. Study map including network stations.

4. Data Processing

Since a wide variety of man-made activities, especially cultural noise, drilling, and pumping exist, the use of polarization can place a high value on noise source determination (Lambert et al., 2011; Lambert et al., 2009; Saadatmand et al., 2013; Saenger et al., 2007c).

In the first step, seismic events were removed from data with the STA/LTA technique. To put it in another way, in order to prevent huge size of unwanted data, the trigger mode was used with a two-second Short Term Average (STA) and a 200-second Long Term Average (LTA) windows. The trigger ratio was eight.

The STA/LTA method is a technique that computes the energy ratio of the short-term average (STA) to long-term average (LTA) of the passive seismic data using a rolling-window. The STA and LTA in the first time window are given by Allen (1978).

$$LTA = \frac{1}{L}\sum_{j=1}^{L} a_j^2 \quad (1)$$

$$STA = \frac{1}{S}\sum_{j=L-S+1}^{L} a_j^2 \quad (2)$$

L and S are the number of data samples in long-term and short-term windows, respectively, and a_j is the amplitude of the j^{th} sample. The STA/LTA ratio, R, is then estimated. After computing R in this window, the window is moved by one sample and the STA/LTA ratio is computed for the new window. For the N^{th} window, the STA and LTA are given by Forghani-Arani et al. (2013).

$$STA_N = \frac{1}{S}\sum_{j=L-S+N}^{L+N-1} a_j^2 \quad (3)$$

$$LTA_N = \frac{1}{L}\sum_{j=N}^{L+N-1} a_j^2 \quad (4)$$

The size of short-term window S depends on the duration of the recorded event that needs to be detected. The size of

the long-term window L can be about five to ten times that of the short-term window.
In data processing, in order to obtain accurate results, about 211 events were detected and removed with the STA/LTA technique, one of which is shown in Figure 2.

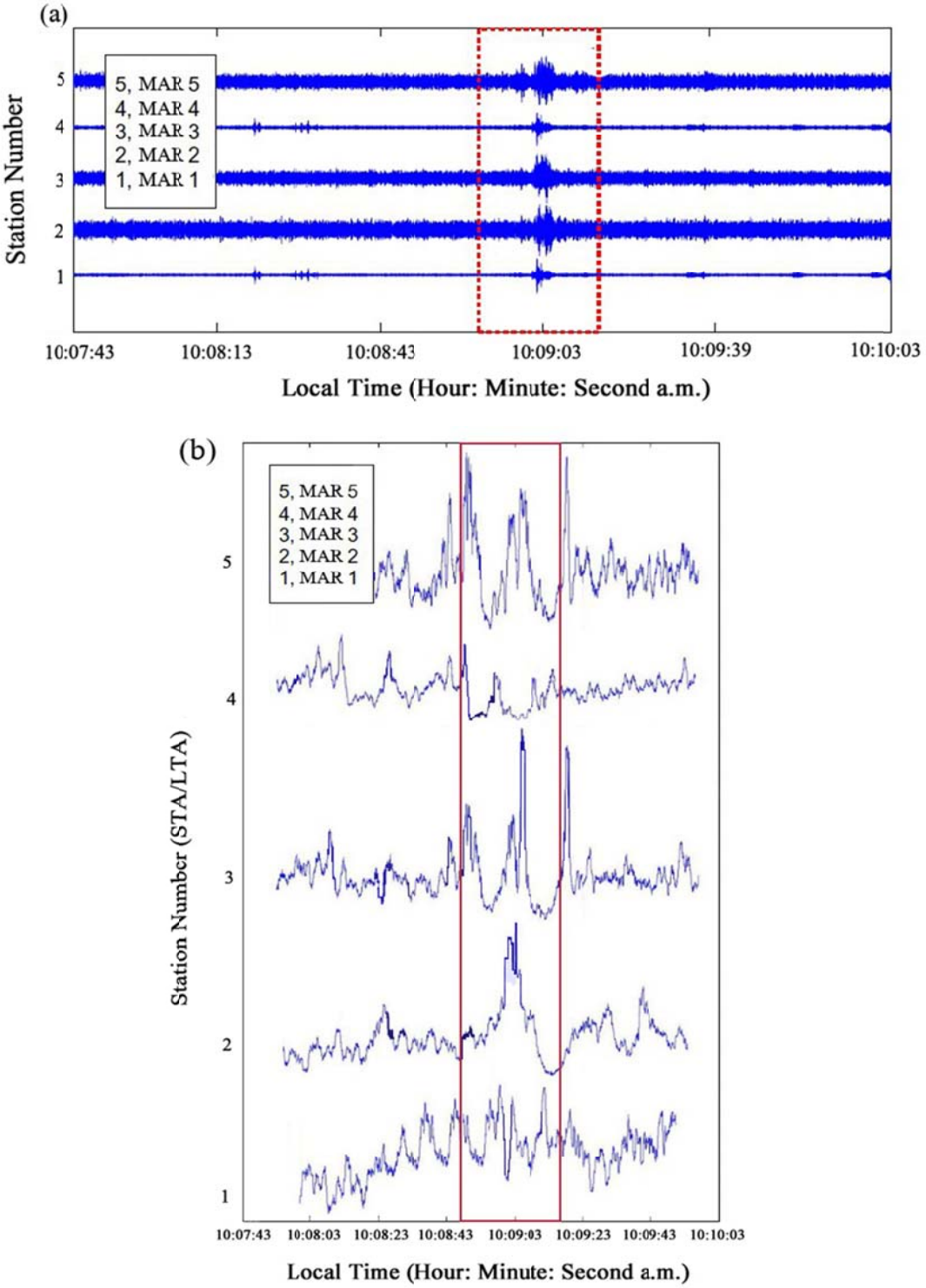

Figure 2. a) Seismogram of an event recorded at the five stations at time 10:09:03 a.m. b) STA/LTA ratios for the stations shows the earthquake event at 10:09:03 a.m.

5. Spectral Analysis

5.1. Vertical-to-Horizontal Spectral ratio

In passive seismic, using Rayleigh-wave energy, several classes of array processing have been reported in the literature over roughly the past 50 years. The simplest processing method is the single station analysis of three-component data to give spectra for the ratio of vertical to horizontal particle motion (Asten, 2006).

Bard (1999) reviewed the method in detail, and it is now widely used for qualitative or semi quantitative mapping of sediment thickness over bedrock, particularly in earthquake hazard zonation studies (Asten, 2006; Bard, 1999; Lachetl and Bard, 1994; Lermo and Chávez-García, 1994). According to Lambert et al. (2009), Vertical-to-Horizontal Spectral ratio (V/H) is considered as an indicator to locate and correlate with the reservoir. This indicator of hydrocarbon potential in seismic waves can be extracted with the analysis of the spectral ratio between vertical records and horizontal ones. V/H spectral ratio in the range frequency of 1-6 Hz is related to the presence of hydrocarbons and in the locations above the reservoir, as it exceeds one. It is shown in the following equations:

$$\frac{V}{H} = \frac{X_V(\omega)}{X_H(\omega)} \tag{5}$$

$$\frac{V}{H} = \sqrt{\frac{2UP^2}{EW^2 + NS^2}} \tag{6}$$

Three possible mechanisms that generate direct hydrocarbon indicator (DHI) in the background spectrum are standing wave resonance, selective attenuation and resonant amplification (Saenger et al., 2007d). The purpose of resonant amplification is that the fluid pressure of reservoirs is increased due to the overburden pressure of rocks over reservoirs. In addition, the size of pores and porosity in reservoir rock decreases with increased overburden pressure. The selective attenuation properties are due to the fact that shear waves cannot propagate through the hydrocarbon, as it is in a state of fluid. The reason is that shear waves do not propagate through the fluid ($\mu = 0$). Nevertheless, body waves propagate through the medium with lower attenuation. That is to say, its primary property is the higher attenuation of shear waves compared with body waves in the fluid mediums. Therefore, propagation of shear waves in such mediums with horizontal components significantly decreases their energy. The impedance contrast between the hydrocarbon and non-fluid medium causes standing wave resonance, which in turn results in reflection (Saenger et al., 2007d).

Regarding the spectral ratio attribute, a trough rather than a peak in the Horizontal/Vertical (H/V) ratio can be found within the range frequency of 1-6 Hz that Dangel et al. (2003) considered for the spectral anomaly related to the hydrocarbon. Therefore, one would develop an attribute using V/H ratio in contrast to the well-known Horizontal-to-Vertical Spectral ratio (H/V) method used by others to identify soil layers with passive seismic data set (Ibs-von Seht and Wohlenberg, 1999; Maresca et al., 2003; Parolai et al., 2004).

In the V/H method, Fourier transform is applied for processed data. Low-frequency passive seismic analysis for locating hydrocarbon reservoir potential is too reliant on the field and survey conditions. It cannot provide accurate information if the field contains noise sources such as industrial and man-made activity because of interference with the hydrocarbon microtremor signal. Thus, further analysis must be performed to avoid misinterpretation. In Figure 3, three results of different methods including V/H Maximum obtained from V/H analysis between 1-6 Hz (Figure 4), seismic section, and geological section are shown together**.** In each station, maximum V/H is shown. In Figures 3.b and 3.c, seismic and geological sections are shown. As can be seen, the best location of the presence of hydrocarbon potential relates to MAR5 station. In Figure 3.b and Fig. 3.c, the circles indicate the trapped oil.

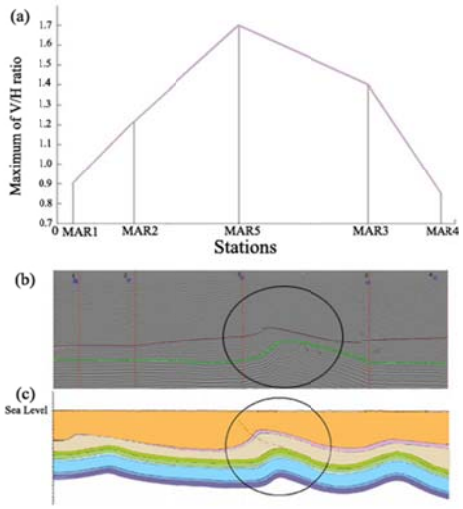

Figure 3. There is a positive correlation among these three results. (a) Maximum of V/H ratio, (b) seismic section, (c) geological section. Figures 3.b and 3.c supplied with courtesy of National Iranian Oil Company (NIOC). The circles show the most probable places for hydrocarbon reservoir from the structural point of view.

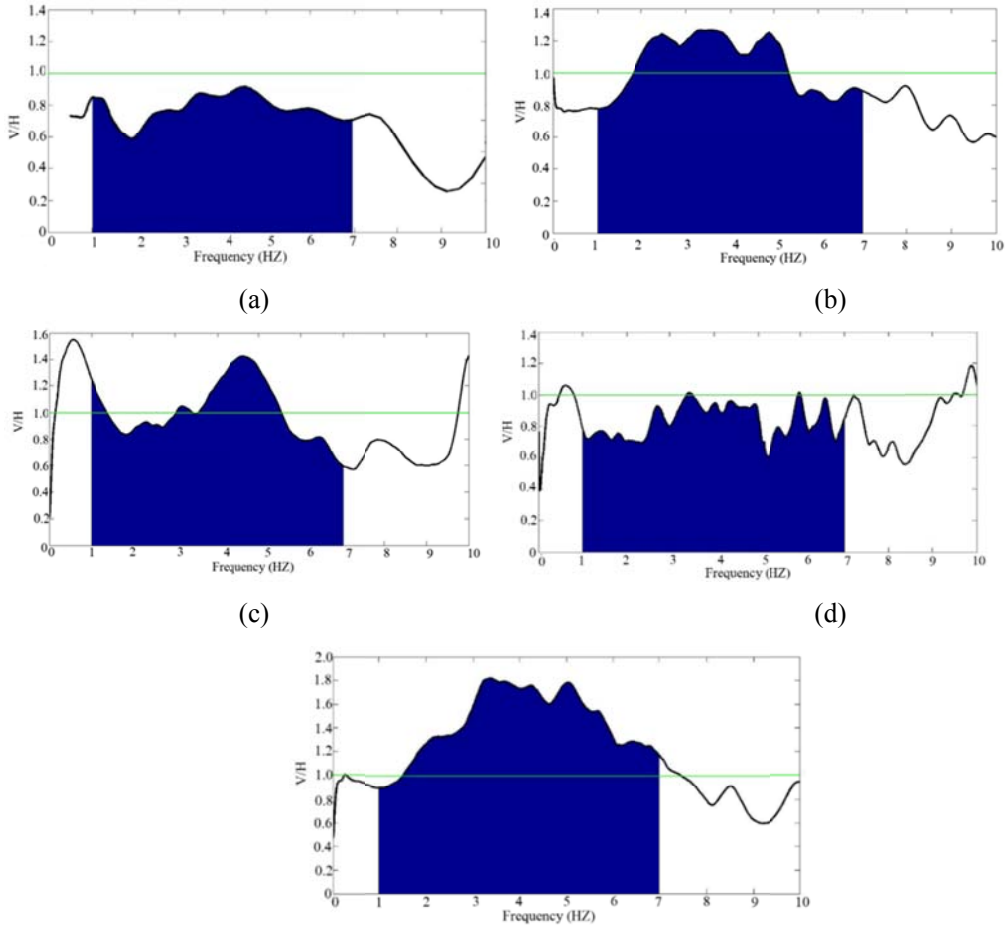

Figure 4. Vertical-to-horizontal spectral ratio diagrams. (a) In MAR1 station, there is no peak in considering frequency (1–6 Hz). (b) In MAR2 station, there is a considerable peak between 2–5.5 Hz in the V/H ratio. (c) In MAR3 station, there is a dominant peak around 3–5.5 Hz in the V/H ratio diagram. (d) In MAR4 station, there is no peak in considering the frequency (1–6 Hz) in the V/H ratio diagram. (e) In MAR5 station, there is a considerable peak between 1.5-6 Hz in the V/H ratio diagram.

5.2 Power Spectral Density (PSD)

Power Spectral Density is equal to power spectral integral under the PSD curve within a frequency band. In terms of processing for PSD, three duration window lengths (before, during, and after the earthquake) is considered 240 seconds for each window that was chosen from 10.03.43 to 10.07.43, 10.07.43 to 10.11.43, and 10.11.43 to 10.15.43 before, during, and after the earthquake respectively, and the PSD attribute of each window is computed.

This attribute is in the low frequency recorded data and is based on the fact that in hydrocarbon potential areas, the energy had been trapped after the earthquake (Fülöp et al., 2016; Saenger et al., 2007c; Stutzmann et al., 2012). This attribute was proposed by Saenger et al. (2007b), which is the process of integration in low frequency spectrum at vertical component called Power Spectral Density.

$$X(\omega)=\int_{-\infty}^{\infty} X(t)e^{-j\omega t}dt \tag{7}$$

$$\text{Average} = \lim_{T\to\infty}\frac{1}{T}\int_{\frac{-T}{2}}^{\frac{T}{2}}\left(X(t)\right)^2 dt \tag{8}$$

$$=\lim_{T\to\infty}\frac{1}{T}\int_{-\infty}^{\infty}\left|x_T(2\pi f)\right|^2 df \tag{9}$$

$$=\int_{-\infty}^{\infty}\lim_{T\to\infty}\frac{\left|x_T(2\pi f)\right|^2}{T}\,df \tag{10}$$

$$=\int_{-\infty}^{\infty} S_X(2\pi f)df \tag{11}$$

$$=s_x(\omega)=\lim_{T\to\infty}\frac{\left|X_T(\omega)\right|^2}{T} \tag{12}$$

To reduce the noise variation, the range frequency was shortened and considered from 1.7-3.7 Hz for this indicator. An earthquake happened on December 26, 2005 at 10:09:03 a.m. (magnitude 4.5 Mb, depth 18 km) was considered. The distance from earthquake epicenter to the network center was about 400 km. The (p-s) arrival time can be derived as the following equation:

$$D = 8\times(Tp-Ts) \tag{13}$$

In Equation (13), $(Tp-Ts)$ is equal to 50 seconds. PSD plots were calculated in three time sections (before, during, and after the earthquake) and are shown in Figure 5. In addition, in each section in order to analyze time sections more accurately, each time sections were considered about 240 seconds, which is 190 seconds after S phase-arrival. It is to be noted in Figure 5 that the color bars show the values of energy.

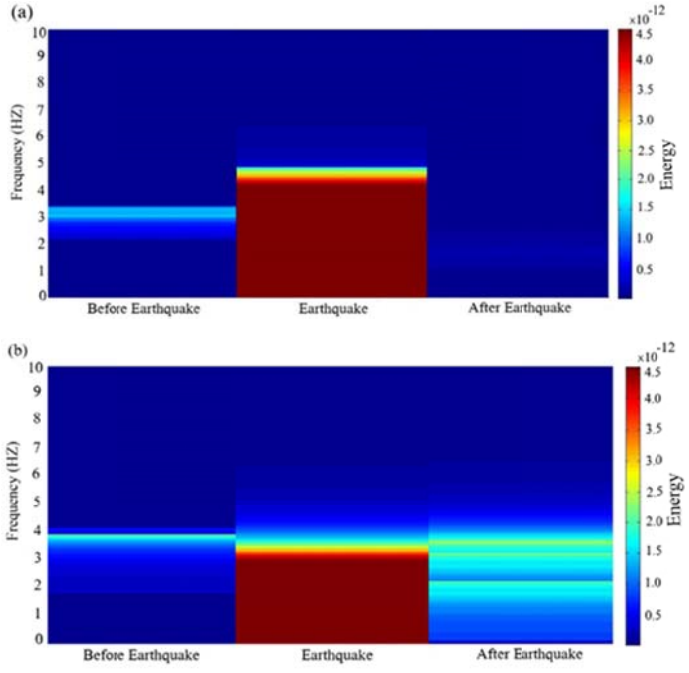

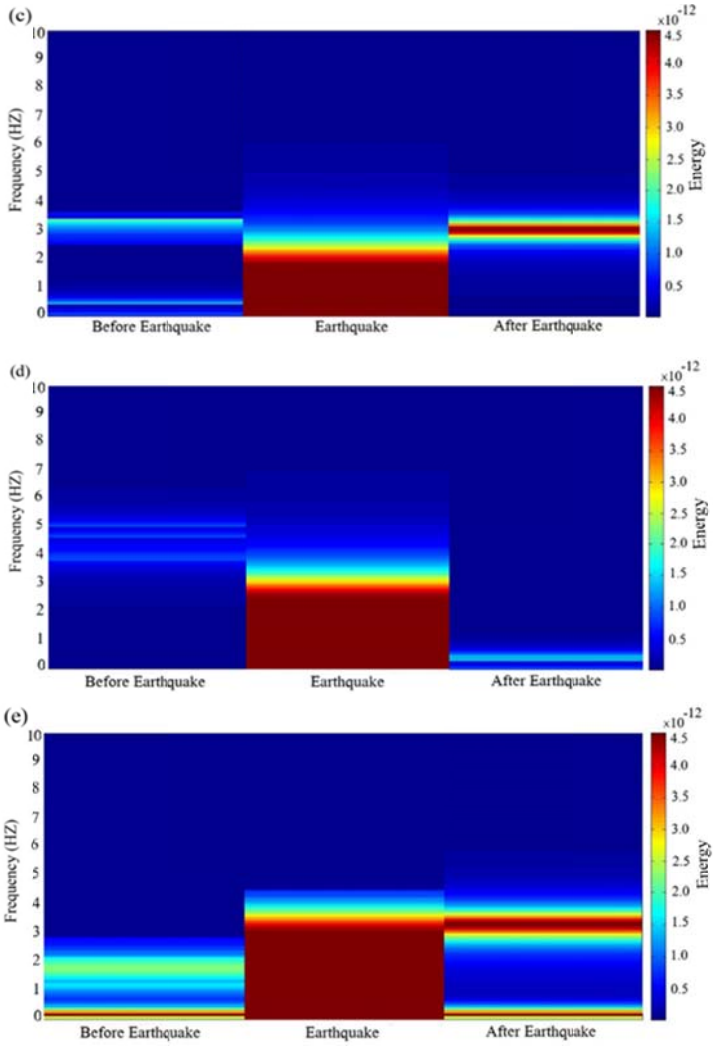

Figure 5. PSD plots for MAR1-5 stations, a) Analysis of PSD in MAR1 station, b) Analysis of PSD in MAR2 station, c) Analysis of PSD in MAR3 station, d) Analysis of PSD in MAR4 station, e) Analysis of PSD in MAR5station.

As it is clear in the color bar, red color presents more energy. In MAR 5 station, the remained energy in the range frequency of 1-6 Hz is much more than the remained energy in MAR1 station.

In MAR1 station, because energy had dropped after the earthquake, there is no hydrocarbon potential. In other words, the remained energy after earthquake is much less than the remained energy before earthquake.

In MAR2 and MAR3 stations, it is expected to have hydrocarbon potential because the energy had been trapped there after the earthquake. However, this trapped energy is insignificant such that it cannot absolutely indicate the absence of hydrocarbon potential, regarding geology and seismic sections. The reason of this anomaly could be its adjacency to MAR5 station having negative effects on MAR2 and MAR3 results.

In MAR 4 station, as can be seen in Figure 5 after the earthquake, in the range frequency of 1-6 Hz, trapped energy cannot be observed in comparison to the condition before the occurrence of the earthquake, because there is no hydrocarbon potential in this area in which geological and seismological studies emphasize.

In MAR5 station, the amount of the energy is expected to reduce after the earthquake. However, the results show that there is a peak at about 4 Hz after the earthquake that indicates hydrocarbon anomaly.

6. Polarization Analysis

As far as any time interval of three-component data are concerned, u_x, u_y and u_z containing N time samples auto- and cross-variances can be obtained by:

$$C_{ij} = \left[\frac{1}{N} \sum_{S=1}^{N} u_i(s) u_j(s) \right] \quad (14)$$

where i and j are the component index x, y, z and s is the index variable for a time sample (Jurkevics, 1988; Saenger et al., 2007c). The 3◊3 covariance matrix

$$C = \begin{pmatrix} C_{XX} & C_{XY} & C_{XZ} \\ C_{XY} & C_{YY} & C_{YZ} \\ C_{XZ} & C_{YZ} & C_{ZZ} \end{pmatrix} \quad (15)$$

is real and symmetric and presents a polarization ellipsoid with best fit to the data. The principal axis of this ellipsoid can be obtained by solving C for its eigenvalues λ_1, $7\lambda_2$ and $7\lambda_3$ eigenvectors p_1, p_2, p_3:

$$(c - \lambda I)P = 0 \quad (16)$$

where I is the identity matrix. The parameter called rectilinearity L, sometimes also called linearity, relates the magnitudes of the intermediate and smallest eigenvalue to the largest eigenvalue:

$$L = 1 - \left(\frac{\lambda_2 + \lambda_3}{2\lambda_1} \right) \quad (17)$$

and measures the degree of how linear the incoming wave field is polarized. It fluctuates between zero and one. The other two polarization parameters describe the orientation of the largest eigenvector $p_1 = (p_1(x), p_1(y), p_1(z))$ in dip and azimuth. The dip can be calculated by:

$$\phi = \tan^{-1} \left(\frac{p_1(z)}{\sqrt{p_1(x)^2 + p_1(y)}} \right) \quad (18)$$

which is zero for horizontal polarization and defined positive in positive z-direction. The azimuth is specified as:

$$\theta = \tan^{-1} \left(\frac{p_1(y)}{p_1(x)} \right) \quad (19)$$

The results of polarization analysis for all five stations are shown in Figure 7.

In Figure 7, the output resulting from analysis of polarization, V/H spectral ratio and three-dimensional modelling come together in order to compare the results of passive seismic noise with each other.

Such figure can help seismologists understand the geologic structure and are a major tool in the exploration and production of oil and gas (Snieder and Wapenaar, 2010).

Wide distribution of particle velocity azimuth using polarization analysis shows that we can trust the results in MAR2, MAR3 and MAR5 stations because the noise is not directional in these stations.

In Figure 7, the fault along the reservoir is located between MAR1 and MAR2 stations and the reservoir structure. According to Figure 7, the mentioned stations are outside the position of the reservoir, which are hundred meters from the southern edge.

Whenever both man-made and artificial noises were removed, four parameters (dip, strength, rectilinearity, and azimuth) of particle motion can be calculated.

According to Saenger et al. (2007a), these parameters have been considered to determine whether or not the area have hydrocarbon. For each station, these parameters were calculated and the results are shown in Figures 8-12 and Table 2. Saenger et al. (2007b) reported that for a measure point with low hydrocarbon potential, dip must be stable, low value ($\approx 20^\circ$) and the strength is relatively low with some spikes. Rectilinearity is lower compared to the values observed above a hydrocarbon reservoir. Azimuth is relatively stable, which could point to an artificial noise source.

Furthermore, in the stations located above hydrocarbon, there are some findings: Dip is stable high value ($\geq 80^\circ$) and this value is directly above the reservoir. Strength is varying. rectilinearity is relatively high and stable and somehow correlated with the strength. Azimuth is strongly varying, as expected for such high dip values.

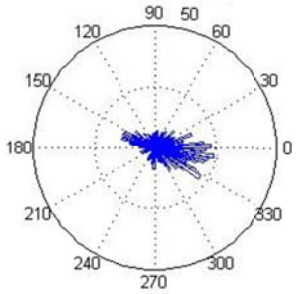

MAR1
MAR1 station is located nearby Maroun anticline at the southwestern edge of the station. As is shown, the azimuth has a slight directivity at the south-East with low eigenvalue.

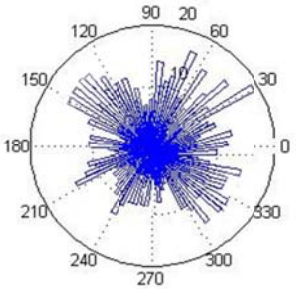

MAR2
MAR2 station is located in low man–made noise area with high eigenvalues and a random directivity.

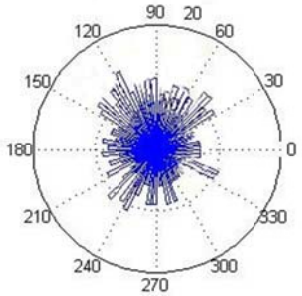

MAR3
MAR3 station is located in low man–made noise area and there is a random directivity in this station.

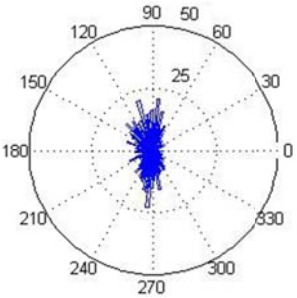

MAR4
MAR4 station is placed with a considerable amount of man–made noise. It is shown that the direction of azimuth is about 25 degree and there is South-North directivity. To top it all, satellite images indicate that this station is situated around a road, which has a negative effect on the data. Thus, windowing is used in several times to reduce high noise.

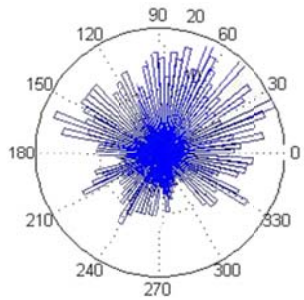

MAR5
MAR5 station is situated in low man–made noise area and directivity is random with high eigenvalue or strong strength.

Figure 6. Results of Azimuth calculation for all stations in December 2005.

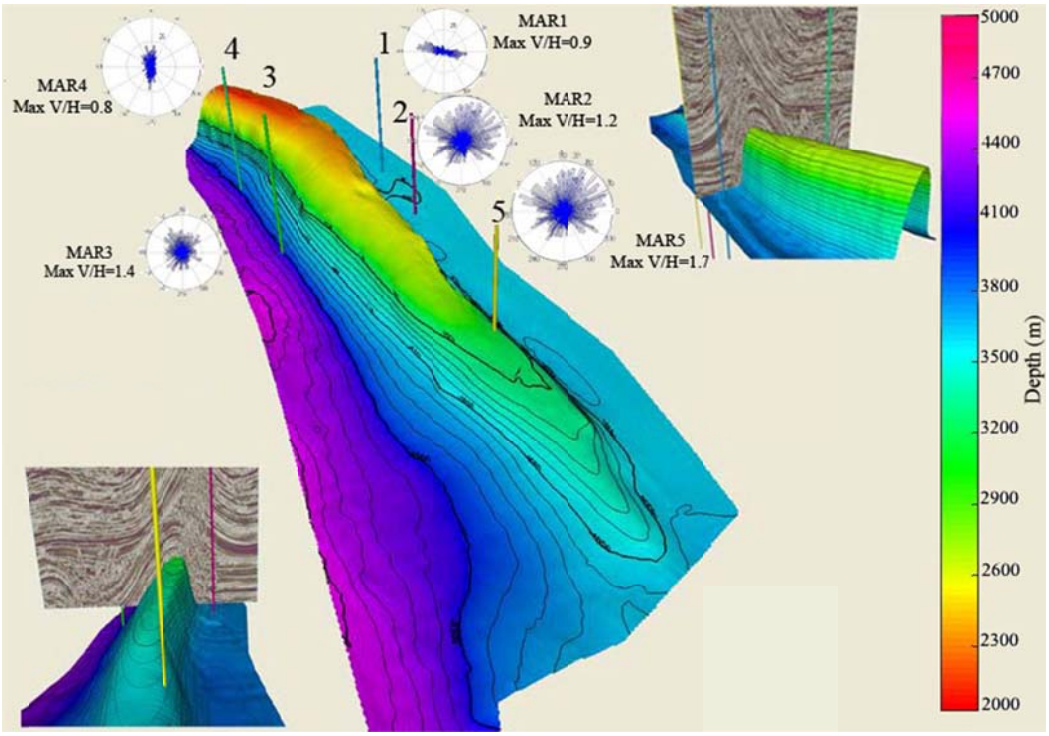

Figure 7. This figure shows Three-dimensional modelling with passive seismic attributes including maximum of V/H spectral ratio and polarization hydrocarbon potential in Maroun oil field. Three-dimensional modelling supplied with courtesy of NIOC. The color bar indicates the increase of depth from 2000 m (red) to 4700 m (purple). In the northern edge, the structure will increase by up to 5000 m. Seismic sections in the location of the stations show thrust fault in the southern edge of the reservoir.

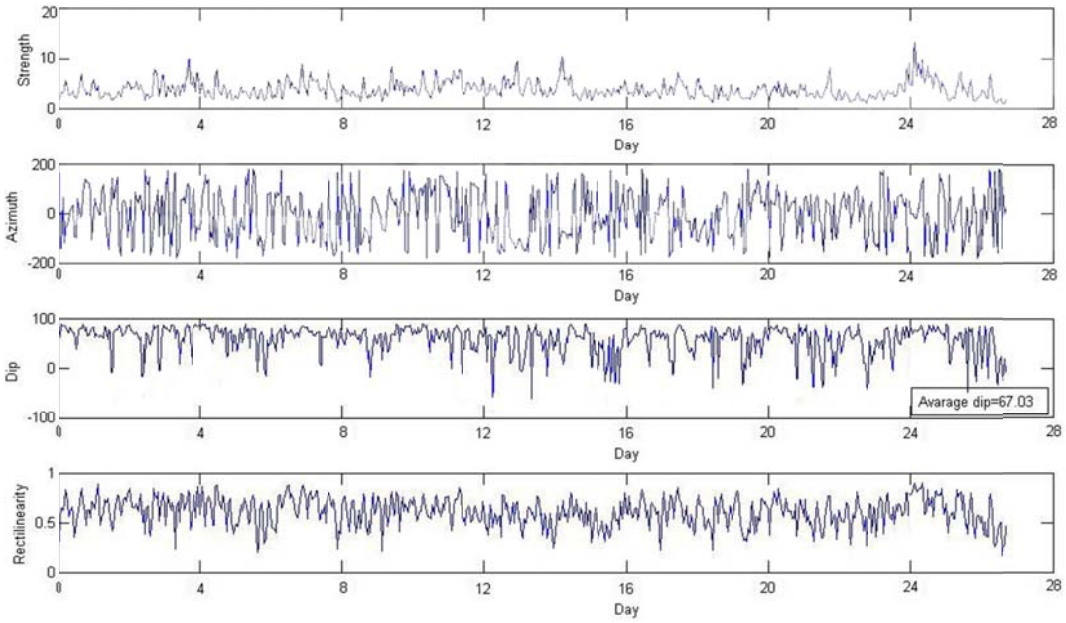

Figure 8. Time variations of strength (λ_1), azimuth (θ), dip (φ) and rectilinearity (L) and from MAR1 station (low hydrocarbon potential). Time unit on the horizontal axes is day-based. The solid line represents the value using data of the whole time period.

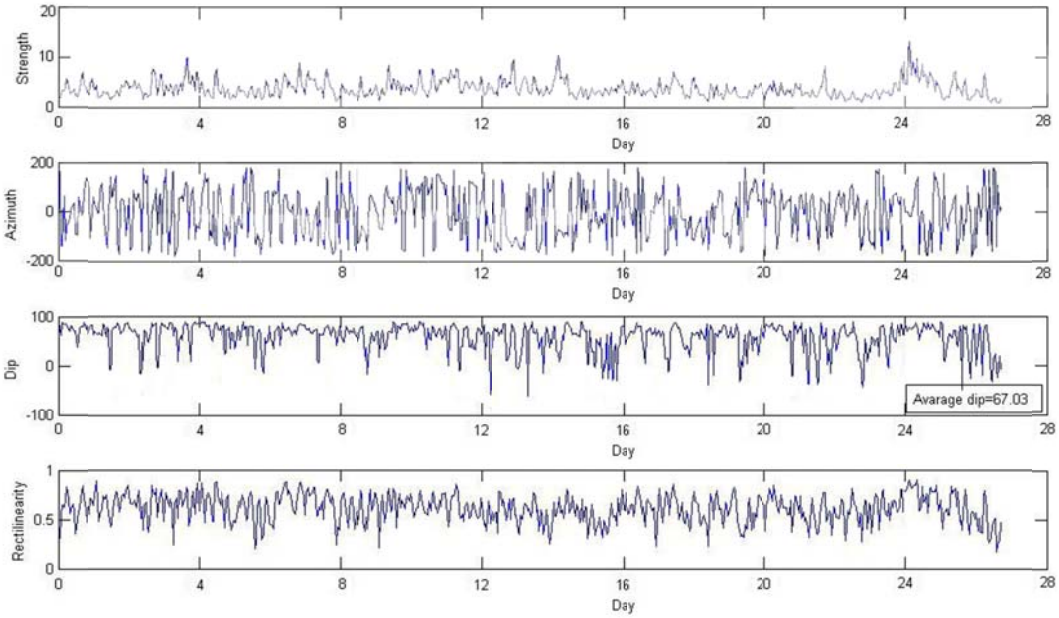

Figure 9. Time variations of strength (λ_1), azimuth (θ), dip (φ) and rectilinearity (L) from MAR2 station (low hydrocarbon potential). Time unit on the horizontal axes is day-based. The solid line represents the value using data of the whole time period.

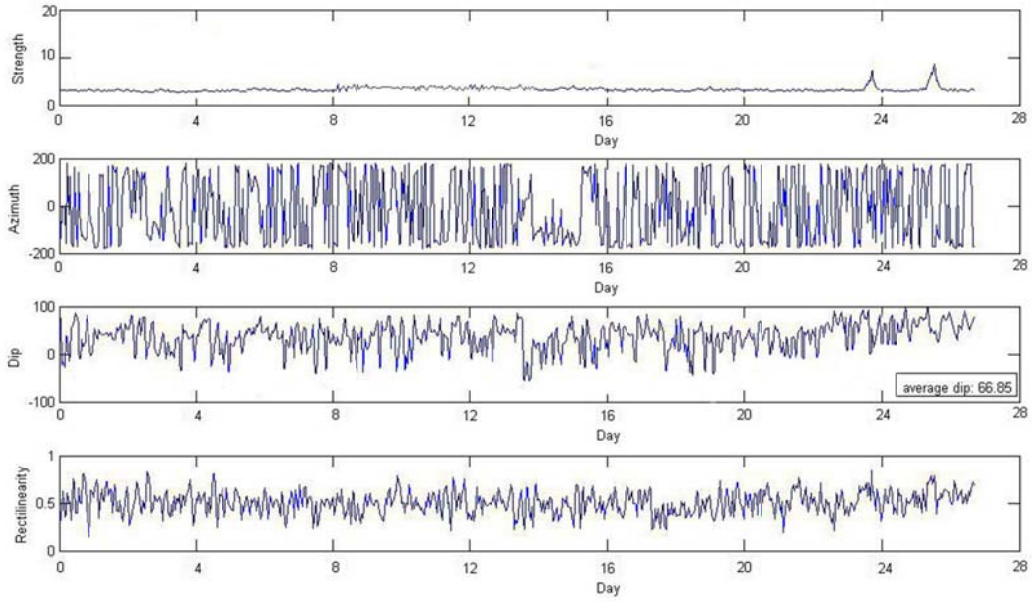

Figure 10. Time variations of strength (λ_1), azimuth (θ), dip (φ) and rectilinearity (L) and from MAR3 station (low hydrocarbon potential). Time unit on the horizontal axes is based on day. The solid line represents the value using data of the whole time period.

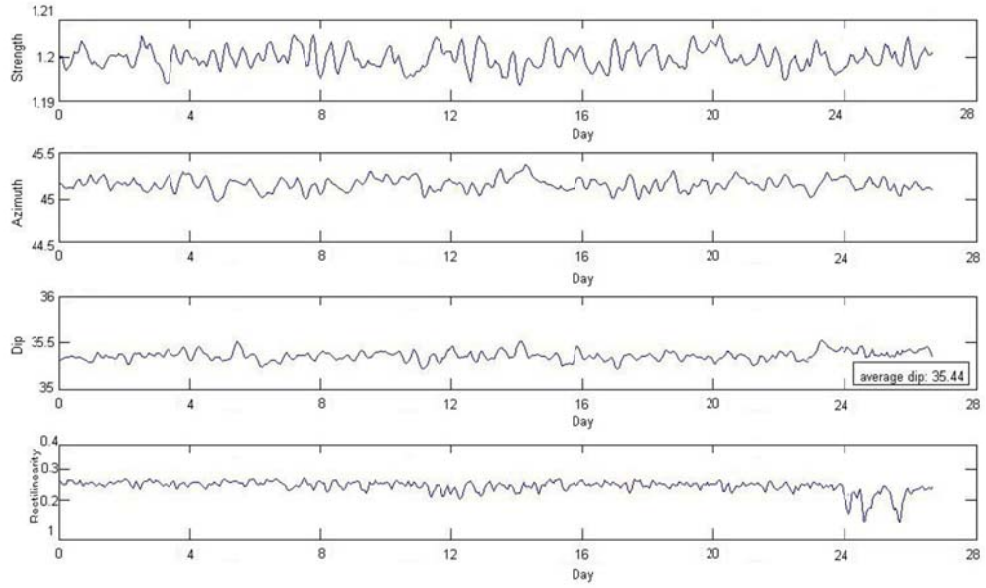

Figure 11. Time variations of strength (λ_1), azimuth (θ), dip (φ) and rectilinearity (L) and from MAR4 station (low hydrocarbon potential). Time unit on the horizontal axes is based on day. The solid line represents the value using data of the whole time period.

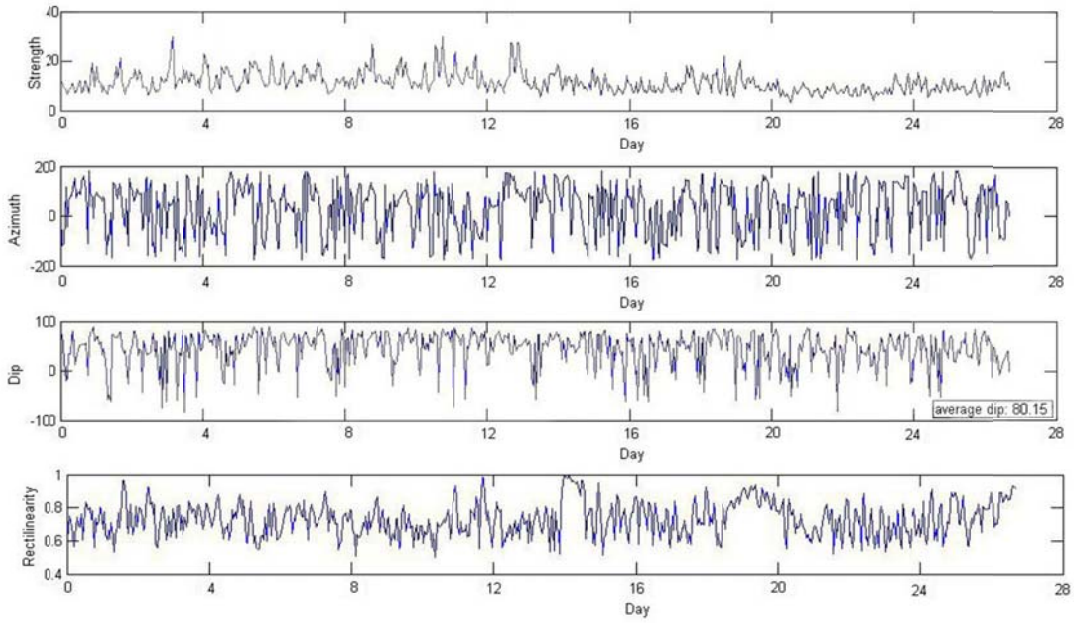

Figure 12. Time variations of strength (λ_1), azimuth (θ), dip (φ) and rectilinearity (L) and from MAR5 station (High hydrocarbon potential). Time unit on the horizontal axes is based on day. The solid line represents the value using data of the whole time period.

Table 2. Comparison of polarization attributes for all stations in Maroun oil field.

STATION	MAR1	MAR2	MAR3	MAR4	MAR5
FIGURE	8	9	10	11	12
DIP	0	67	68	35	80
AZIMUTH	Relatively Stable	Unstable between -200 and 200	Unstable between -200 and 200	Stable about 45	Unstable between -200 and 200
LARGEST EIGENVALUE (STRENGTH)	low	Relatively low	Relatively low	Relatively low with some spikes	Varying, but relatively high during measurement period
RECTILINEARITY	The measurement is below 0.5	Relatively high	The measurement is over 0.5	Fluctuating between 0.2 and 0.3	Relatively high

Table 2 shows four polarization parameters including dip, azimuth, strength and rectilinearity. With regard to the aforementioned, polarization characteristics were analyzed in order to find the presence or absence of hydrocarbon, the results of which are as follows: In MAR5 station, all of the polarization parameters show the presence of hydrocarbon. MAR4 station results do not show the presence of hydrocarbon because they do not have any indicator of hydrocarbon potential. In MAR2 and MAR3 stations, some indicators show the presence of hydrocarbon such as azimuth, while other indicators such as dip show the absence of hydrocarbon. It seems that there is paradox in the interpretation of polarization results that is due to the adjacency to MAR 5 station.

In order to remove the high noises in the data of MAR4 station, windowing is used up to the point that the desired data are usable.

Table 3 shows the probability of hydrocarbon potential based on the type of indicator (number one is high probability of hydrocarbon reservoir and number zero represents very low probability of hydrocarbon reservoir). The possibility of hydrocarbon potential is shown in four categories ranging from Very low to High.

7. Conclusions

It is clear that the analysis of polarization in this paper has very strong correlation with the result of three-dimensional seismic experiment. As to last geophysics works, in particular seismic reflection survey, the earlier results about Maroun oil field and Spectral methods adapt to the polarization results in this passive seismic experiment.

In this paper, polarization analysis, has successfully revealed the results. In this study, MAR5 station is located over hydrocarbon reservoir. As a result, MAR2 and MAR3 stations are situated nearby hydrocarbon reservoir. Besides, MAR1 and MAR4 stations are deprived of hydrocarbon anomaly. This research shows that in Maroun region V/H spectral ratio and PSD indicate reservoir location.

Regarding Table 3, the best location for hydrocarbon reservoir is related to MAR5 station having a complete certainty of hydrocarbon potential with the use of different geophysical methods.

As to seismic section in Figure 3, the result reports that the medium probability in MAR 2 and MAR 3 stations in comparison with MAR5 station. Consequently, MAR 2 and MAR 3 stations are less likely to have hydrocarbon potential. In MAR1 and MAR4 stations, all performed geophysical methods reject the presence of hydrocarbon potential because there is a clear directivity in our data.

Table 3. The Possibility of hydrocarbon potential with various geophysical methods.

Station	V/H	PSD	Polarization	Possibility
MAR1	0	0	0	Very low
MAR2	1	1	0	Medium
MAR3	1	1	0	Medium
MAR4	0	0	0	Very low
MAR5	1	1	1	High

Acknowledgements
Authors would like to express their appreciation to the National Iranian Oil Company (NIOC) for their full cooperation and providing the data required for the current study.

References

Allen, R. V., 1978, Automatic earthquake recognition and timing from single traces. Bulletin of the Seismological Society of America, 68(5), 1521-1532.

Asten, M., 2006, On bias and noise in passive seismic data from finite circular array data processed using SPAC methods. Geophysics, 71, 153–162.

Bard, P.-Y., 1999, Microtremor measurements: a tool for site effect estimation: The effects of surface geology on seismic motion, 3, 1251-1279.

Berberian, M., 1981, Active faulting and tectonics of Iran: Zagros Hindu Kush Himalaya Geodynamic Evolution, 33-69.

Berberian, M., 1986, Seismotectonics and earthquake-fault hazard study of the Karkheh river project: Jahad-e-Sazandegi, Tehran, p. 180.

Berberian, M., 1995, Master "blind" thrust faults hidden under the Zagros folds: active basement tectonics and surface morphotectonics, Tectonophysics, 241(3), 193-224.

Dangel, S., Schaepman, M., Stoll, E., Carniel, R., Barzandji, O., Rode, E.-D. and Singer, J., 2003, Phenomenology of tremor-like signals observed over hydrocarbon reservoirs: Journal of Volcanology and Geothermal Research, 128(1), 135-158.

Forghani-Arani, F., Behura, J., Haines, S. S. and Batzle, M., 2013, An automated cross-correlation based event detection technique and its application to a surface passive data set: Geophysical Prospecting, 61(4), 778-787.

Fülöp, L., Jussila, V., Lund, B., Fälth, B., Voss, P., Puttonen, J., Saari, J., Heikkinen, P. and Oy, Å.C., 2016, Modelling as a tool to augment ground mo-tion data in regions of diffuse seismicity-Progress 2015.

Gerivani, H., Haghshenas, E., Moghaddas, N. H. and Ghafoori, M., 2012, Frequency–amplitude range of hydrocarbon microtremors and a discussion on their source. Journal of Geophysics and Engineering, 9(6), p. 632.

Holzner, R., Eschle, P., Zürcher, H., Lambert, M., Graf, R., Dangel, S. and Meier, P., 2005, Applying microtremor analysis to identify hydrocarbon reservoirs. First Break, 23(5).

Ibs-von Seht, M. and Wohlenberg, J., 1999, Microtremor measurements used to map thickness of soft sediments: Bulletin of the Seismological Society of America, 89(1), 250-259.

Jackson, J., 1980, Reactivation of basement faults and crustal shortening in orogenic belts.

Jackson, J. and Fitch, T., 1981, Basement faulting and the focal depths of the larger earthquakes in the Zagros mountains (Iran), Geophysical Journal International, 64(3), 561-586.

Jackson, J. and McKenzie, D., 1984, Active tectonics of the Alpine-Himalayan Belt between western Turkey and Pakistan, Geophysical Journal International, 77(1), 185-264.

Jurkevics, A., 1988, Polarization analysis of three-component array data. Bulletin of the Seismological Society of America, 78(5), 1725-1743.

Lachetl, C. and Bard, P.-Y., 1994, Numerical and theoretical investigations on the possibilities and limitations of Nakamura's technique. Journal of Physics of the Earth, 42(5), 377-397.

Lambert, M.-A., Nguyen, T., Saenger, E. H. and Schmalholz, S. M., 2011, Spectral analysis of ambient ground-motion-Noise reduction techniques and a methodology for mapping horizontal inhomogeneity. Journal of Applied Geophysics, 74(2), 100-113.

Lambert, M. A., Schmalholz, S. M., Saenger, E. H. and Steiner, B., 2009, Low-frequency microtremor anomalies at an oil and gas field in Voitsdorf, Austria. Geophysical Prospecting, 57(3), 393-411.

Lermo, J. and Chávez-García, F. J., 1994, Are microtremors useful in site response evaluation?. Bulletin of the seismological society of America, 84(5), 1350-1364.

Maresca, R., Castellano, M., De Matteis, R., Saccorotti, G. and Vaccariello, P., 2003, Local site effects in the town of

Benevento (Italy) from noise measurements. Pure and Applied Geophysics, 160(9), 1745-1764.

Marzorati, S. and Bindi, D., 2006, Ambient noise levels in north central Italy. Geochemistry, Geophysics, Geosystems, 7(9).

Parolai, S., Richwalski, S. M., Milkereit, C. and Bormann, P., 2004, Assessment of the stability of H/V spectral ratios from ambient noise and comparison with earthquake data in the Cologne area (Germany). Tectonophysics, 390(1), 57-73.

Peterson, J., 1993, Observations and modeling of seismic background noise.

Saadatmand, M. R., Moradi, A. and Hashemi, H., 2013, Passive seismic survey on the Darquain oil field. Journal of Tethys, 1(3), 215-224.

Saenger, E. H., Schmalholz, S., Podladchikov, Y., Holzner, R., Lambert, M., Steiner, B., Quintal, B. and Frehner, M., 2007a, Scientific strategy to explain observed spectral anomalies over hydrocarbon reservoirs generated by microtremors, in Proceedings 69th EAGE Conference and Exhibition incorporating SPE EUROPEC 2007.

Saenger, E. H., Torres, A., Rentsch, S., Lambert, M., Schmalholz, S.M. and Mendez-Hernandez, E., 2007b, A hydrocarbon microtremor survey over a gas field: Identification of seismic attributes, SEG Technical Program Expanded Abstracts 2007, Society of Exploration Geophysicists, 1277-1281.

Saenger, E. H., Torres, A., Rentsch, S., Lambert, M., Schmalholz, S. M. and Mendez, H., 2007c, A hydrocarbon microtremor survey over a gas field: Identification of seismic attributes. Proceedings 77th SEG meeting, San Antonio, Texas, USA, Expanded Abstracts 2007c, 1277-1281.

Saenger, E. H., Steiner, B., Schmalholz, S., Lambert, M., Quintal, B., Frehner, M. and Podladchikov, Y., 2007d, Considerations of observed spectral anomalies over hydrocarbon reservoirs generated by microtremors, Proceedings 10th International Congress of the Brazilian Geophysical Society & EXPOGEF 2007, Rio de Janeiro, Brazil, 19-23 November 2007, Society of Exploration Geophysicists and Brazilian Geophysical Society, 1144-1149.

Snieder, R. and Wapenaar, K., 2010, Imaging with ambient noise: Physics Today, 63(9), 44-49.

Stutzmann, E., Ardhuin, F., Schimmel, M., Mangeney, A. and Patau, G., 2012, Modelling long-term seismic noise in various environments, Geophysical Journal International, 191(2), 707-722.

Walker, D., 2008, Recent developments in low frequency spectral analysis of passive seismic data, First Break, 26(2).

Webb, S. C., 2007, The Earth's 'hum'is driven by ocean waves over the continental shelves, Nature, 445(7129), 754-756.

Wilson, D., Leon, J., Aster, R., Ni, J., Schlue, J., Grand, S., Semken, S., Baldridge, S. and Gao, W., 2002, Broadband seismic background noise at temporary seismic stations observed on a regional scale in the southwestern United States, Bulletin of the Seismological Society of America, 92(8), 3335-3342.

Young, C. J., Chael, E. P., Withers, M. M. and Aster, R. C., 1996, A comparison of the high-frequency (> 1 Hz) surface and subsurface noise environment at three sites in the United States. Bulletin of the Seismological Society of America, 86(5), 1516-1528.